Observations of wall conditioning by means of boron powder injection in DIII-D H-mode plasmas

A. Bortolon[1], R. Maingi[1], A. Nagy[1], J. Ren[2], J. D. Duran[2], A. Maan[2], D. C. Donovan[2], J. A. Boedo[3], D. L. Rudakov[3], A. W. Hyatt[4], T. W. Wilks[5], M. W. Shafer[6], C. M. Samuell[7], M. E. Fenstermacher[7], E. P. Gilson[1], R. Lunsford[1], D. K. Mansfield[1], T. Abrams[4], R. Nazikian[1] and the DIII-D team

[1] *Princeton Plasma Physics Lab., 100 Stellarator Rd, PO Box 241, Princeton, NJ 08543 USA*

[2] *University of Tennessee Knoxville, Knoxville, Tennessee 37996, USA*

[3] *University of California, San Diego, California 92093, USA*

[4] *General Atomics, PO Box 85608, San Diego, California 92186, USA*

[5] *Massachusetts Institute of Technology, Plasma Science and Fusion Center, Cambridge, MA 02139, USA*

[6] *Oak Ridge National Laboratory, Oak Ridge, Tennessee 37831, USA*

[7] *Lawrence Livermore National Laboratory, Livermore, California 94550, USA*

abortolon@pppl.gov

Abstract

We report observations from the DIII-D tokamak indicating that boron (B) powder injection in tokamak plasmas improves wall conditions similarly to glow discharge boronization. Isotopically enriched B powder (B^{11}>95%) was introduced gravitationally in a sequence of H-mode plasma discharges at rates up to ~160 mg/s for durations up to 3 s. Boron injection to cumulative amounts ≤0.1 g appeared to improve wall conditions similarly to boronization, with indications of reduced wall fueling, reduced recycling at the outer strike point and reduced impurity content at breakdown. Post-mortem analysis of graphite samples exposed to far scrape-off layer (SOL) plasma fluxes during boron injection confirm the formation of a B-C layer, with average surface composition B:C~1. The results suggest that injecting boron-rich powders in tokamak plasmas can effectively replenish boron films on carbon plasma facing components to improve wall conditions and extend the duration of the beneficial effects of glow discharge boronization.

1 Introduction

The performance of present-day magnetic confinement fusion devices depends strongly on the conditions of the plasma facing components (PFCs), which can act as uncontrolled sources of impurities through chemical and physical processes, and of the main fuel gas through recycling. Different techniques have been explored and developed to minimize these effects and allow operation with controlled density and low impurity concentrations [1]. The most commonly used procedure is glow discharge boronization (GDB), which consists of chemical deposition of boron (B) coatings by means of prolonged glow discharges using boron rich gases such as diborane, B_2D_6, or trimethylboron, $B(CH_3)_3$. As a practical example, a boronization in the DIII-D tokamak [2] currently starts as a D_2 or He glow discharge, into which diborane gas (B_2D_6) is introduced in concentrations up to 20% [3]. During the GDB, the machine walls are maintained at a temperature of ~300ºC to enhance desorption of deuterium and impurities and form better quality layers. In these conditions, GDB allows to grow B-rich coatings of ~100 nm thickness in ~4-8 hours, resulting in approximately 10-20 g of B deposited on the wall. This procedure provides a uniform coating of the main chamber walls and the lower divertor volume [4], which in DIII-D is relatively open. The beneficial effects related to global reduction of oxygen and deuterium desorption last up to approximately 100 plasma discharges (500 s of plasma), in conjunction with between shots glow, after which a new GDB might be required.

GDB was initially developed at TEXTOR [5] and subsequently implemented in virtually all presently operating fusion devices [6], enabling robust plasma breakdown and operation with reduced impurities and wall fueling. The good wall conditions provided by GDB have expanded the tokamak operation parameter space, leading to the discovery of high performance H-mode regimes [7], [8], and reliable execution of plasmas at low collisionality [9].

While GDB has matured into a reliable and effective technique for wall conditioning in present-day devices, this technique does not directly extrapolate to long pulse, next-step fusion devices, where static magnetic fields from superconducting coils would prevent the use of glow discharges between plasma shots, and, more importantly, the coatings would saturate and/or erode within a small number of long pulse plasmas.

This motivated the research of alternative ways of replenishing the B-rich coatings, in particular through injection of B in tokamak plasma discharges, using B-rich gases or solid B compounds [6]. Different techniques have been explored, including plasma fueling with B-rich

gases [10], erosion of B-coated limiters [11] and injection of solid, B-containing particles [12], [13]. Perhaps the most prominent example of in-shot deposition of low-Z coatings remains in the Tokamak Fusion Test Reactor (TFTR) experiments, where lithium and boron pellets injected in the early phase of plasma discharges provided the reduced recycling needed to achieve high fusion yield in the second part of the discharge when neutral beams (NB) were engaged [12], [14].

In this work we report results from recent experiments in DIII-D, investigating the potential of B powder injection during tokamak operation as a method to complement and extend the benefits of GDB. To our knowledge, the use of B powder for in-situ wall conditioning was first attempted in Alcator C-Mod (molybdenum PFCs) [13], where elemental B powder of 50-100 μm particle size was injected gravitationally with a dedicated, solenoid-driven injector. The experiments did not provide clear evidence of assimilation of B by the plasma, nor did they find positive effects on plasma operation, possibly due to substantial erosion preventing the growth of coatings of relevant thickness [15]. More recently, similar experiments were executed in ASDEX-Upgrade, now with full tungsten wall, using a newly installed impurity powder dropper (IPD), developed by Princeton Plasma Physics Laboratory [16]. In the experiments, B and boron nitride (BN) powder were injected gravitationally into high-density, H-mode plasmas with the goal of regenerating B coatings specifically on the limiters of the ion cyclotron resonance frequency (ICRF) antenna, which represent strong source of tungsten sputtering when the antenna is operated [17]. The injection of B-rich powders resulted in reduced sputtering of oxygen and tungsten from the limiters, allowing execution of low density plasmas required to obtain suppression of edge-localized modes (ELMs) with externally-applied magnetic perturbations without prior GDB [18].

In this work, we report the results of a companion experiment carried out in the DIII-D tokamak as a part of the commissioning of the IPD system installed in Spring 2018. The experiment provided indications of stepwise improvements in plasma parameters correlating with B powder injection and measurements of the chemical characteristics of the actively deposited B-rich film.

The remainder of this manuscript is organized as follows: Section 2 provides an overview of the experimental tools and experiment chronology; Section 3 illustrates the effect of B injection on plasma operation; Section 4 assesses wall conditioning effects in early phase of plasma

discharges where the shot-by-shot comparison is not confounded by the effects of ELM activity; Section 5 is devoted to the surface analysis of graphite samples exposed to plasma flux during B powder injection; and finally Section 6 discusses the results in a broader context and identifies gaps that future studies would need to address to understand and further develop the potential of the technique.

2 Experiment overview

Experimental tests of the wall conditioning effect of B powder injection were carried out as part of DIII-D start-up operation after a two-day machine vent to atmosphere. Approximately 40 deuterium plasma cleaning discharges with various magnetic equilibria and plasma shapes preceded the B injection experiment to promote desorption of impurities (water, oxygen nitrogen) and deuterium from the graphite PFCs. The machine start-up was executed with plasma current directed with the toroidal magnetic field, i.e., opposite to the standard field helicity for DIII-D, in preparation of the subsequence physics experiments requiring low density plasmas and counter current neutral beam injection. This initial clean-up activity amounted to approximately 200 s of plasma operation with P_{NBI}=4-12 MW. Additionally, 6-8 minute He glow discharges were performed between plasmas.

The real-time wall conditioning experiment was conducted in five consecutive plasma discharges with B powder injected during the plasma current flat-top phase. The effectiveness of wall conditioning was inferred from the shot-by-shot evolution of observables such as the neutral pressure and impurity emission.

Figure 1(a) illustrates the magnetic configuration utilized for the experiment, which corresponds to the ITER-baseline shape at B_t=-1.7 T, I_p=-1 MA, P_{NBI}=7 MW [19]. In this LSN magnetic configuration, both B_t and I_p are clockwise if viewed from the top. The outer strike point is positioned in proximity to the cryo-pump baffle to allow effective removal of the desorbed gas and facilitate density control. For this experiment the cryo-pump was kept at liquid helium temperature.

B injection was performed using the impurity powder dropper (IPD) [16]. The device delivers a continuous flow of B powder at calibrated rates between 2-200 mg/s. This experiment used commercially available B powder with mesh-100 (granule size 40-100 μm, mass between ~0.1-5 μg). Boron powder isotopically enriched to >95% B^{11} was chosen to facilitate the analysis of deposited layers, allowing to discriminate the injected B from natural B already present on the wall from GDB (natural B consists of 19.8% B^{10}, 80.2% B^{11}). The B powder is delivered to the plasma gravitationally through a vertical drop tube whose location (major radius R=1.485 m) is indicated in Figure 1(a). In this magnetic configuration, assuming free fall in vacuum the powder is expected to reach the separatrix at a speed of ~10 m/s. Single-particle estimates of the ablation times [20] suggest that the particles of the injected size range ablate in the near SOL, i.e., close to

the separatrix. However, deeper penetration might occur due to a local reduction of the electron temperature associated with the ablation and ionization of injected powder, as well as radiative cooling. Figure 1(b) shows an image captured by a wide-angle visible camera [21], which during this experiment was configured to collect C-III emission through a narrow band filter centered at 465 nm (2 nm FWHM). The toroidal section of DIII-D covered by this diagnostic field of view (toroidal machine angle φ~115-190°) does not include the IPD injection location (φ=195°). Nevertheless, an emerging plume is visible from behind the central column, expanding towards the viewer. The plume, which is attributed to emission from He-like B-IV at 465.8 nm transmitted by the diagnostic bandpass filter, appears to expand toroidally in the direction opposite to the plasma current up to ~60° from the injection location (1.5 m in the toroidal direction). Assuming that the plume expansion is predominantly aligned with the local magnetic field, this expansion is poloidally directed towards the outer target. No measurements were available to ascertain whether the plume also extends in the opposite direction. A similar plume was clearly observed during B injection in ASDEX Upgrade by wide-angle cameras, expanding along field lines unidirectionally from the ablation region in the direction of the plasma current [22]. However, the magnetic field helicity was opposite the DIII-D case, so the plume expansion was poloidally directed towards the inner target.

The Divertor and Midplane Material Evaluation Systems (DiMES and MiMES, [23]) were used to quantitatively evaluate wall coating effects through ex-situ analysis of graphite samples exposed to divertor/midplane plasma. The locations of DiMES and MiMES are indicated in Figure 1(a). In the chosen magnetic configuration both systems were exposed to far-SOL plasma with values of the normalized poloidal flux ψ_N=1.04-1.06. The samples were introduced before the first plasma with B injection and retracted two discharges after the last plasma with B injection. As such, their analysis provides information on the cumulative effect from multiple discharges with IPD. As part of commissioning the IPD system, short-pulse, low rate test drops using both B and Li powder were also performed at the end of plasma discharges at the beginning of the day. The amount of powder injected in these tests amounted to <1 mg of for both impurities, that is much smaller than what used for subsequent injections for wall conditioning and deemed non-perturbative for these studies.

During the DIII-D machine start-up only diagnostics strictly required for plasma operation are operational. This includes measurements of plasma density with interferometry, impurity

emission from the vacuum ultra-violet spectrometer SPRED and various neutral pressure gauges. Measurements of kinetic profiles (electron and ion temperature and density) from diagnostics such as Thomson scattering and charge-exchange recombination spectroscopy were unavailable for this experiment. A detailed analysis of the effects of impurity injection on profiles or plasma stability is thus deferred to future studies.

3 Effect of boron injection on plasma operation

B powder injection (BPI) was carried out during a sequence of successive plasma discharges at relatively low rates of ~10 mg/s for time intervals of 1-3 s. The injection parameters are indicated in Table 1. Figure 2 illustrates the chronological sequence of plasma discharges, including two discharges prior to B injection. The evolution of the BPI is shown by the blue curves in Figure 2, which represent the calibrated rate measured by the IPD flow meter [16], here shown with a 0.8 s delay to indicate the approximate time of ablation into the plasma accounting for the powder free-fall time. Boron powder injection aided in achieving reproducible, full-duration plasmas during machine start-up. As is typical during start-up plasmas following a manned-entry vent, plasmas suffered from impurity accumulation, magneto-hydrodynamic (MHD) instabilities, and uncontrolled density. These effects lead to irregular, sparse ELMs, ELM-free phases, and early discharge terminations. This was the case for several consecutive discharges including 176706 where a locking n=1 mode causes loss of H-mode, and 176707, where a large n=2 mode results in a long ELM-free phase with an uncontrolled density increase leading to disruption at t~3 s after approximately 1 s of I_p flat-top. In the following discharge (176708), a 1 s injection of B powder was applied from t=2.0 s. The resulting discharge showed a longer I_p flat top up to t=3.5 s. In the following two discharges (176709, 176710) B injection was applied at approximately the same rate but for a 3 s duration, resulting in the end of the programmed flat top at t=5 s. Injection at a much higher rate (120 mg/s) was attempted in the successive shot (176711) but resulted in an almost immediate disruption. This completed the B injections for the day, which continued with the successful execution of 12 full-duration plasmas without BPI. These observations suggest a correlation between the duration of plasma flat-top and BPI and appear to be closely related the presence of ELMs, which are known to provide effective control of density and prevent impurity accumulation [24]. In fact, although during BPI

the ELMs vary in character and frequency, BPI still appears to promote ELMs. This might be associated with fluctuations in the powder deposition rate, providing local, impulsive perturbations of the pedestal which act as “seed” for instabilities. BPI might also increase in collisionality (from the higher Z_{eff}) could also result in a pedestal more prone to ballooning instabilities [25].

Another interesting observation is that the L-H transition occurs at progressively later times with the introduction of B (Table 1), consistent with an increase of the L-H power threshold. This is associated with a shot-by-shot reduction of the plasma density achieved in the L-mode phase, which is discussed further in the next section.

4 Evaluation of wall conditions during L-mode phase

Since the ELM behavior varies substantially in this series of plasma discharges, it is challenging to infer the effect of the changing wall conditions from the plasma parameters in the flat-top phase. To that end, in this section, we focus the analysis on the early evolution of these plasma discharges from plasma breakdown until t=500 ms. Over this time interval the plasma remains in L-mode, no B injection is applied, and the magnetic configuration is still evolving (in terms of B_t, I_p, and plasma shape). After the breakdown the plasma is limited on the central wall until the diverted shape reaches its target configuration at t=320 ms, shown in Figure 1(a). In this configuration the outer strike-point (OSP) is located on the divertor floor close to the lower cryo-pump baffle.

4.1 Wall fueling

Figure 3 shows the evolution of the plasma current, I_p, neutral beam injected power, P_{NBI}, line-averaged electron density, n_e, and deuterium Balmer-α brightness, D_α along a chord monitoring the OSP. The curves are color-coded according to the cumulative amount of B powder injected in prior discharges. The evolution of n_e remains qualitatively similar throughout the series: n_e increases monotonically until t=320 ms when the OSP is positioned close to the crypo-pump baffle; then n_e rolls over due to efficient divertor cryogenic pumping and stabilizes at a lower value, $n_{e,l}$ which represents the stationary density of the L-mode phase. A clear step-wise reduction of the L-mode density is visible in the shot-by-shot evolution. Before beginning B injections (blue curves) $n_{e,l}$~$4x10^{19}$ m^{-2} and does not change significantly shot by shot, indicating that the wall conditions are saturated or evolving slowly. Conversely, after the first injection of B the time evolution of n_e follows a lower trajectory to a smaller peak, resulting in a substantial density reduction ($n_{e,l}$~$2.5x10^{19}$ m^{-2}), which decreases weakly with increasing amount of B injection. A step-wise reduction is also observed in the D_α emission from the OSP [Figure 3(c)], which decreases by a factor >60% after the first B injection. Unfortunately, lack of n_e and T_e measurements on the lower divertor floor (e.g., from Langmuir probes) prevents the determination of whether the reduction of D_α emission is representative of a reduction of deuterium recycling from the wall.

A general reduction of wall fueling is seen by inspecting the time history of the feedback-controlled plasma fueling. In these discharges D_2 gas was fueled through a valve located on top of the machine [Figure 1(a)]. The valve was activated according to a pre-programmed waveform up to t=200 ms after which the density feedback control was engaged. Figure 4(a) compares the experimental evolution of the plasma density with the target value programmed. Before beginning B injection the experimental density exceeds the target, even after the gas valve is shut off at 320 ms by the feedback control. This is a clear indication of fueling dominated by wall desorption. Conversely, after the first injection of B, the plasma density remains close to the requested density, with the gas valve opened by the feedback control to compensate for values lower than the request. In subsequent shots, similar values of L-mode density were obtained by applying consistently higher gas fueling. This clearly indicates the effect of wall pumping is correlated with BPI in the early phase of the plasma discharge.

A reduction of the wall fueling was also suggested by measurements of the neutral gas pressure at various locations in the vacuum vessel using high accuracy, ASDEX-style, hot-cathode ionization gauges [26]. For t>50 ms, i.e. after the peak associated with plasma breakdown, the main chamber pressure at the outer equatorial plane, remains <0.1 mPa [Figure 4 (c)]. While this pressure is at the limit of the instrument accuracy, clear qualitative changes are visible after the beginning of B injection because the measured amplitudes fall below the detection threshold. The pressure measured in the cryo-pump plenum [Figure 4 (d)] is more significant for t>300 ms when the OSP is positioned near the pump baffle. For discharges after B injection, the plenum pressure decreases from ~3.4 to ~1 mPa in this phase. Interestingly, when considering the three shots executed after the first B injection one can notice a progressive 50% reduction of plenum pressure from 2.4 to 1.2 mPa. At the same time, the small reduction of electron density (5%) suggests that divertor target particle fluxes are not changing substantially. Therefore, it is concluded that the observed reduction of neutral pressure is primarily caused by a global increase of D retention in the wall.

4.2 Impurities

The reduction of wall impurity sources is a key element of wall conditioning. Figure 5 shows the evolution of the brightness of selected C, O and N lines measured by the core vacuum ultra-

violet spectrometer SPRED [27]. These lines (C IV 38.4 nm, O IV 55.5 nm, N IV 92.3 nm) are emitted by ion charge states that exist primarily in the plasma edge and are thus not directly informative of the "deep-core" impurity content, but nevertheless are typically used to ascertain the state of the DIII-D walls. In particular, the peak brightness at breakdown is used as a metric to qualify the wall conditions during machine startup. During the sequence of discharges under examination, a stepwise reduction of the peak amplitude of C-IV, O-IV and N-V emission at breakdown was observed, down to values ~50% smaller than those before B injection. The brightness of these lines does not show strong variation after B injection, indicating the persistence of the BPI wall conditioning effect.

Figure 5(d) shows the brightness of the Ni XVIII line at 29.2 nm, whose breakdown peak is also clearly reduced after B injection. After t=300 ms the Ni emission is dominated by pulses which correlate with modulation of the heating NB, indicating a strong contribution from charge-exchange recombination. The 'active' charge-exchange contribution corresponds to emission from the plasma center, where the SPRED chord intersects the heating beam neutrals. This active emission pulses are observed to decrease in amplitude with subsequent exposures to B, indicating a reduction of Ni density in the plasma core.

The core impurity content can be also investigated with line-integrated measurements of visible bremsstrahlung (VB) along chords that intersect the plasma core. This is shown in Figure 5(e) where a clear reduction of the VB brightness is observed for t>300 ms. While this reduction is consistent with a reduction in effective charge Z_{eff}, it can be mostly attributed to the reduced electron density. Conversely, when the plasma is inboard limited in the time interval t=200-300 ms, plasmas after B injection show higher VB emission at lower n_e, suggesting higher impurity concentrations. This could be associated with residual B powder mobilized by the plasma formation.

4.3 Shot-by-shot evolution of wall conditions

Figure 6 summarizes the shot-by-shot evolution of selected quantities indicative of the wall conditions over an extended range of eight plasma discharges. For each quantity, the values at breakdown (t=30-60 ms) and during the diverted, L-mode phase (t=470-500 ms) are indicated. A vertical line indicates the separation between plasma startups before and after the first B

injection, which took place during the flat-top of all plasmas starting from shot 176708. The data series shows clear changes in trends correlated with the beginning of B injections. This is particularly clear for the brightness of C-IV and O-IV lines at breakdown in Figure 6(d), and for C-III line emission from the OSP in Figure 6(c,g). It should be noted that these indications of reduced impurity content or source are not conclusive, however, since a reduction of electron density is concurrent with the reduction of impurity line emission.

The observations of constant density sustained with larger gas fueling and lower pumping suggest an increase D retention in the wall, presumably associated with a fresh B-rich layer deposited during BPI. The D retention rate has been estimated computing a dynamic particle balance [28] by accounting for the known particle sources (gas valves, neutral beams) and sinks (pump). Figure 7 shows the D retention rate inferred for the sequence of shots in analysis in the time interval t=350-450 ms. In this time window all plasmas in the series are in similar conditions, i.e. L-mode, diverted configuration, with significant OSP pumping and slowly varying density, allowing a more robust particle balance estimate. The results of the particle balance calculation in this time interval indicate that before BPI the D retention rate was <0.1 Pa m^3/s and slightly negative for shot 176708, which followed a plasma disruption. Conversely, after BPI a larger rate of 0.4 Pa m3/s is found, increasing linearly up to 1.0 Pa m^3/s in the two subsequent shots. These values are of the same order of the gas injection rates in this time window [(Figure 4(b)], indicating that an increase of D wall retention to values sufficient to affect the global particle balance, resulting in effective wall pumping during the L-mode diverted phase.

5 Surface analysis of DiMES and MiMES samples

The results shown in the previous section indicate that BPI in DIII-D H-mode plasmas resulted in a stepwise change of plasma parameters during the current and density ramp-up. The critical question is whether these changes are associated with changes of wall conditions, and specifically with B coating effects. A simple upper bound estimate can be carried out to determine whether the injected amounts are sufficient to deposit a layer of non-negligible thickness, by assuming that all B powder injected is fully deposited in form of pure B (mass density 2.46 g/cm^3), with uniform thickness on the divertor surface (10 m^2). In that case, BPI at 10 mg/s results in a B layer growing by 1 nm/s, i.e., a coating efficiency of 0.1 nm/mg of injected B (for pure B, 1 nm corresponds to ~5 monolayers). This estimate indicates that injections at rates and durations used in the experiment are appropriate for growing B layers on the divertor PFC of thickness of a few nm - smaller but comparable to a typical GDB [6]. Extending the surface of B deposition to include areas of the main chamber wall, for instance associated with ELMs, would reduce the estimated layer thickness.

As discussed above, graphite deposition samples were exposed to plasma for the entire duration of the experiment using the DiMES [29] and MiMES [23] probes. For these experiments, a flat, pristine graphite cap 4.8 cm in diameter was mounted on DiMES with its plasma facing surface aligned flush with the lower divertor tiles 20 cm radially outboard of the OSP (ψ_N~1.06-1.09). The MiMES probe was configured with four pristine graphite sample buttons inserted on a cylindrical graphite head. The latter featured an oblique poloidal profile conforming to the local flux surface tilt and a toroidally wedged profile [30], with one half of the probe nominally parallel to the magnetic flux surface (buttons 1 and 2), and the other exposed to downstream fluxes with magnetic field line incidence angles of 7° (buttons 3 and 4). During exposure MiMES was inserted with its surface protruded few millimeters beyond the limiter shadow. DiMES and MiMES were positioned at their collection location at the beginning of the experimental sequence (before shot 170701) and retracted after shot 176713, for a total of 12 plasma exposures. Note that, due to machine access constraints, two additional shots without B powder injection were executed after the last BPI exposure in shot 176711, After those the samples were retracted. In principle, this allowed for potential spurious effects due to erosion and redeposition from the additional exposure to plasma without B injection. Nevertheless, in the magnetic configuration utilized, both samples were exposed to the far SOL, where plasma flux is

typically low but expected to increase substantially during BPI due to B powder ablation in the open field line region. Considering that B sputters more effectively than D, it is reasonable to expect that the surface dynamics at the sample locations will be largely determined by plasma fluence during BPI.

Figure 8 shows photographs of the samples after plasma exposure, including discolorations indicative of stronger plasma-material interaction. Ex-situ analysis of the collected samples with Laser Ablation Mass Spectroscopy (LAMS) [31] and X-ray photoelectron spectroscopy (XPS) [32] conclusively found layers of B associated with the powder injection. The LAMS technique consists of ablating the DiMES head with a laser in a series of rows across the sample surface. Craters produced by the laser can be up to 1 μm deep, much deeper than the expected deposition layer thickness. During ablation, the liberated particles are swept to a mass spectrometer by a helium carrier gas. The traveling species are measured for isotopic B content by a quadrupole mass spectrometer. The resulting data can be used to construct bi-dimensional maps of the relative isotopic concentration on the sample surfaces.

Figure 9 shows the map of the B^{11} and B^{10} concentrations found with 2-D LAMS analysis of the DiMES cap. Both isotopes were detected across the entire sample surfaces with signal well above noise level. Localized regions of higher-than-background signal emerge with a similar pattern for both species. Consequently, despite these localized structures, the ratio between the measured intensity of B^{11}/B^{10} remains relatively constant across the surface [Figure 9(c)]. Because the relative magnitude of the signal is indicative of isotopic abundance, this result indicates B^{11} is ~98% of the total B distributed uniformly across the analyzed surface. This provides conclusive evidence that the B deposited on the sample largely originated from the injected powder. Notice that the structures in the deposited B layer do not correlate with the tokamak radial direction, suggesting that B fluxes to the sample in the far-SOL are present, but with weak radial dependence. Furthermore, the scale of these structures is small compared to the typical radial SOL scale lengths [33], suggesting that they may be associated with pre-existing non-uniformities on the sample surface.

LAMS analysis of MiMES buttons also found B^{11} enrichment levels consistent with the injected material (B^{11}>95%) for both downstream and upstream exposed buttons. The enrichment level only depended weakly on the location and orientation of the laser ablation scan (Figure 10). Contrary to expectations, larger B concentrations are found on buttons 3 and 4 that

were exposed to upstream fluxes, i.e., directed from the outer divertor target to the equatorial plane, opposite to expected direction of the ablated B. This counter-intuitive result might be the effect of stronger erosion of the deposited layer on buttons 1 and 2 (exposed to downstream fluxes), possibly in the plasmas executed after the last BPI shot. This indicates a complex dynamic of deposition and erosion which might take place on timescales comparable to few plasma discharges.

XPS analysis of the DiMES surface was also carried out to determine the composition of the surface layer. XPS measurements were performed at ten equally spaced locations along a central segment cut from DiMES in the machine radial direction. The results shown in Figure 11(a) indicate that the surface is composed of approximately 40% C, 40% B, and 18% O and 2% Li, all with weak or negligible spatial dependence. The Li content is likely associated with a small test Li injection at the beginning of the experimental day. Conversely, the O content can be attributed to water vapor in the residual vacuum and especially from the sample exposure to air between the experiment and the analysis. Note that XPS measurements are surface sensitive with a probe depth of <10 nm and hydrogenic species are undetectable. The relative elemental composition of B and C at the surface layer is measured to be approximately B:C~1:1 uniformly across the DiMES cap diameter. Notice that the XPS measurement collects signal from a relatively large area of ~0.4 mm diameter, that is much larger than the spatial scales of the surface morphology (profilometry scans yielded surface roughness R_a~5 μm, consistent with a hand-polished surface). Therefore, the measured elemental abundances should be interpreted as averages over small-scale inhomogeneous distribution pattern of B deposits in the rough graphite surface.

Since the XPS measurements are sensitive to the first few monolayers of the material, repeated, timed irradiation of the samples with a 1 keV Ar ion beam was used to probe progressively deeper surface layers and determine the elemental composition as a function of the sample depth. Figure 11(b) shows the elemental composition as a function of the sputtered depth. The results show a surface layer of constant composition approximately 1 nm thick. For increasing depth, the concentration of B and O decrease monotonically but relatively high concentrations (>10%) are found down to 15 nm below the sample surface. This relatively deep detection could be associated with the sample surface roughness rather than actual implantation or diffusion into the bulk material. It could also be the result of ion beam mixing due to the Ar

sputtering beam [34], which promotes diffusion of surface atoms into deeper layers. This effect steadily increases with increasing sputter fluence so that the accuracy of the XPS measurement is strongly reduced at larger depths. Considering these limitations, the XPS measurements indicate that the thickness of deposited B-rich layer can vary in the range of 1-15 nm.

While the dominant fraction of the O was likely adsorbed under atmospheric exposure during the weeks between the experiment and sample surface analysis, it is interesting to observe that the relative elemental concentration of B and O remains approximately constant across the depth profile, B/O~2.3. This suggests that the O content is directly linked to chemical bonding with the deposited B and not with C. This is consistent with the typical O gettering properties observed for GDB [1]. This also suggests that the amount of O that can be gettered has reached saturation at all depths. The chemical composition of the B-O compounds was not studied in this sample. Previous studies have measured formation of boron oxides upon irradiation of B-C materials with energetic O ions in the form of BO, B_2O, B_2O_2, B_2O_3 as well as non-stoichiometric B-O bonds (see [6], [35] and references therein).

The ex-situ DiMES characterization can be used for a crude estimate of the coating efficiency. We consider, as a reference, that a B-rich film of thickness ~10 nm (consistent with the XPS measurements depth profile measurements) is obtained after a cumulative injection of 95 mg of B over 7 s with an average mass injection rate of 14 mg/s (see Table 1). Under these conditions, we infer a boronization film growth efficiency of ~0.1 nm/mg of injected B. In other words, an injection rate of 10 mg/s, well within the capabilities of the IPD system, yields a film growth rate of 1 nm/s. This growth rate is consistent in magnitude with the estimate reported at the beginning of this section, assuming a uniform deposition in the divertor region. This suggests that the hypothesis that the injected material is mainly deposited in the divertor region is reasonable. However, it is important to remark that these coarse estimates are based on local measurements at the DiMES location and that the dynamics of film growth will depend strongly on the poloidal location of the surface within the tokamak.

6 Discussion and outlook

We report DIII-D start-up experiments where during a sequence of H-mode plasma discharges a step-wise reduction of wall fueling was observed after injection of elemental B in

the form of powder, indicating a positive wall conditioning effect. The concomitant reduction of impurity radiation also suggests a reduction of impurity wall sources, but in the absence of detailed measurements it is impossible to disentangle the effects of the reduced plasma density and reduced impurity sourcing on the brightness of impurity lines. The observed changes were obtained with injection of very modest quantities of B (<200 mg cumulative) compared with a standard GDB, which typically leaves ~10-20 g of B deposited onto the PFCs. In particular, the step-wise improvements in wall conditions found after the first 10 mg of B injected did not continue with successive injection, suggesting a possible saturation of the relevant surfaces.

The results from the surface analysis of graphite samples exposed to the divertor and main chamber SOL with the DiMES and MiMES probes allow an initial assessment of the effectiveness of the BPI technique to coat graphite PFCs in comparison with the commonly applied GDB. GDB typically can grow a B-rich coating layer at rates of 0.05 nm/s [6] depending on the glow discharge characteristics such as pressure, bias, the type of B-rich gas, and the carrier gas (D_2, He) [3]. The layer thickness at the end of a GDB increases with the duration of the procedure up to a maximum of a few hundreds of nm. The C:B ratio in the deposited layer typically varies between 0.5 and 2 (see Ref. [6] and references therein), but high purity can also be achieved; analysis of the deposits after the first DIII-D boronization found a layer 150 nm thick with B concentration >90% [3].

In the case of BPI, our observations from PFCs exposed to the far SOL indicate a much faster growth rate of ~1 nm/s, but, due to the short exposure times, a smaller layer thickness. In a graphite machine as DIII-D, the PFC layer is not pure but appears to consist of a B-C amorphous compound of relative concentration B:C~1:1 uniformly across the sample (non-uniformities might exist at surface roughness scales). This value is consistent with reports from GDB in graphite wall machines, for instance in TEXTOR [5] and ASDEX-Upgrade [36]. We conjecture this ratio to be the result of differential erosion leading to a final elemental composition that minimizes sputtering yield. This would be the case if domains of the surface with a B-C ratio richer in B or in C displayed a higher erosion rate than corresponding domains with B:C=1:1. In this regard, it is interesting to note that erosion yields by hydrogen flux lower by a factor up to 10–20 have been documented for films with a ratio B:C~1:1 compared to amorphous C [1]. Erosion during between-shot He glows could also contribute to this effect. New experiments are in progress to confirm and elucidate this aspect. While mechanisms of this kind would limit the

purity of the B layer achievable in a C wall machine, they would also imply weak dependence on the magnitude of the B fluxes to the wall and, hence, a more uniform layer composition. Although the O found in the BPI grown layer is attributed to air exposure, an O gettering behavior similar to GDB [6] was documented. The amounts of elemental O that can be sequestrated appear to saturate to a level of approximately 1 O atom per 2.3 B atoms (O:B~0.4).

Adsorption of D in the deposited B-rich layers provides an natural explanation for the observed changes in particle balance illustrated in Section 4.1, consistent with the well-documented the ability of a-B/C:H and BCOD films to retain hydrogen isotopes more effectively compared with carbon (see Ref. [6] and [37] and references therein). This is typically quantified by surface analysis techniques such as thermal desorption spectroscopy. In this case, however, since the sample's exposure to air was expected to alter the hydrogen inventory, this analysis has not been pursued.

The experimental results illustrated in this work, together with those from the ASDEX-Upgrade tokamak with full W wall [18], [22], represent a promising first step in the investigation of the viability of B powder injection as a wall conditioning method which does not require interruption of plasma operation. This technique may have important applications in the operation of long-pulse or steady-state devices where B coatings will be subject to rapid erosion and long-term evolution of the PFCs can become a factor limiting plasma performance. Moreover, the BPI could be an attractive method for present-day fusion machines, since in contrast with GDB (i) it does not involve handling of hazardous, toxic and/or explosive gases, (ii) it can be applied without interrupting physics operations, and (iii) it is compatible with static magnetic fields from superconducting coils. To demonstrate viability for next-step long-pulse devices several important questions need to be addressed. These primarily concern:

1. The distribution of the coating layer across the machine wall, which is expected to depend on plasma scenario (e.g. ELMs, SOL width, detachment) and can potentially be used to optimize the deposition at specific locations.
2. The layer chemical and physical properties, which vary depending on the PFC material (C, W, Be) and B powder injection program (rate, duration).
3. The robustness of coatings against erosion during long plasma operations or changes of magnetic field configuration.

4. Potential flaking of thick accumulated layers, with consequent generation of erosion dust, whose amount pose strict limits the operation of a large-scale fusion reactor [38], [39].
5. The stability and duration of beneficial effects, in particular with regard to reduction of sputtering sources and fuel recycling.
6. The retention of hydrogenic species in the coating layers, in particular with regard to the control of tritium inventory in a fusion reactor [40].

Dedicated experiments in DIII-D and ASDEX-Upgrade are planned to quantify the structure of B-rich deposited layers, for instance with respect to the distance from the strike-points, and quantify the duration of the impurity reduction effects. Experiments planned in long pulse machines as the stellarator LHD, where an IPD has been recently installed [41], [42], will be deliver key information on long term robustness and stability. At the same time, interpretative modeling of the experimental results can be leveraged to understand the complex, multi-physics dynamics at play during BPI in tokamak plasmas. Integrated modeling efforts, combining different simulation tools to resolve the physics of B powder migration/ablation, SOL transport of B to the targets, and plasma surface interaction processes is in progress and will be the subject of future publications.

Acknowledgments

This material is based upon work supported by the U.S. Department of Energy, Office of Science, Office of Fusion Energy Sciences, using the DIII-D National Fusion Facility, a DOE Office of Science user facility, under Awards DE-FC02-04ER54698 (GA), DE-AC02-09CH11466 (PPPL), DE-FG02-07ER54917 (UCSD), DE-AC52-07NA27344 (LLNL), DE-AC05-00OR22725 (ORNL), and DE-SC0014264 (MIT).

Disclaimer: This report was prepared as an account of work sponsored by an agency of the United States Government. Neither the United States Government nor any agency thereof, nor any of their employees, makes any warranty, express or implied, or assumes any legal liability or responsibility for the accuracy, completeness, or usefulness of any information, apparatus, product, or process disclosed, or represents that its use would not infringe privately owned rights. Reference herein to any specific commercial product, process, or service by trade name, trademark, manufacturer, or

otherwise does not necessarily constitute or imply its endorsement, recommendation, or favoring by the United States Government or any agency thereof. The views and opinions of authors expressed herein do not necessarily state or reflect those of the United States Government or any agency thereof.

References

[1] J. Winter, "Wall conditioning in fusion devices and its influence on plasma performance," *Plasma Phys. Control. Fusion*, vol. 38, no. 9, pp. 1503–1542, Sep. 1996, doi: 10.1088/0741-3335/38/9/001.

[2] J. L. Luxon, "A design retrospective of the DIII-D tokamak," *Nucl. Fusion*, vol. 42, no. 5, p. 313, May 2002, doi: 10.1088/0029-5515/42/5/313.

[3] J. Phillips *et al.*, "Initial boronization of the DIII–D tokamak," *J. Vac. Sci. Technol. A Vacuum, Surfaces, Film.*, vol. 10, no. 4, pp. 1252–1255, Jul. 1992, doi: 10.1116/1.578235.

[4] G. L. Jackson *et al.*, "Boronization in DIII-D," *J. Nucl. Mater.*, vol. 196–198, pp. 236–240, Dec. 1992, doi: 10.1016/S0022-3115(06)80038-3.

[5] J. Winter *et al.*, "Boronization in textor," *J. Nucl. Mater.*, vol. 162, no. C, pp. 713–723, Apr. 1989, doi: 10.1016/0022-3115(89)90352-8.

[6] O. I. Buzhinskij and Y. M. Semenets, "Review of in Situ Boronization in Contemporary Tokamaks," *Fusion Technol.*, vol. 32, no. 1, pp. 1–13, Aug. 1997, doi: 10.13182/FST97-A19875.

[7] G. L. Jackson *et al.*, "Regime of very high confinement in the boronized DIII-D tokamak," *Phys. Rev. Lett.*, vol. 67, no. 22, pp. 3098–3101, Nov. 1991, doi: 10.1103/PhysRevLett.67.3098.

[8] C. M. Greenfield *et al.*, "Quiescent Double Barrier Regime in the DIII-D Tokamak," *Phys. Rev. Lett.*, vol. 86, no. 20, pp. 4544–4547, May 2001, doi: 10.1103/PhysRevLett.86.4544.

[9] W. Suttrop *et al.*, "Experimental conditions to suppress edge localised modes by magnetic perturbations in the ASDEX Upgrade tokamak," *Nucl. Fusion*, vol. 58, no. 9, p. 096031, Sep. 2018, doi: 10.1088/1741-4326/aace93.

[10] H. . Esser, V. Philipps, H. . Reimer, and P. Wienhold, "Plasma discharge fuelling by trimethylboron-a new wall conditioning technique," *Nucl. Fusion*, vol. 32, no. 2, pp. 278–

281, Feb. 1992, doi: 10.1088/0029-5515/32/2/I08.

[11] C. Boucher *et al.*, “Comparison of three boronization techniques in TdeV,” *J. Nucl. Mater.*, vol. 196–198, pp. 587–591, Dec. 1992, doi: 10.1016/S0022-3115(06)80104-2.

[12] J. A. A. Snipes *et al.*, “Wall conditioning with impurity pellet injection on TFTR,” *J. Nucl. Mater.*, vol. 196–198, no. 0, pp. 686–691, Dec. 1992, doi: http://dx.doi.org/10.1016/S0022-3115(06)80123-6.

[13] J. Irby *et al.*, “Elemental Boron Injector for Wall Conditioning on the Alcator C-Mod Tokamak,” *Proc. Annu. Meet. APS Div. Plasma Phys.*, 2003, [Online]. Available: https://www-internal.psfc.mit.edu/research/alcator/pubs/APS/aps2003/IrbyPoster.pdf.

[14] J. D. Strachan *et al.*, “Wall conditioning experiments on TFTR using impurity pellet injection,” *J. Nucl. Mater.*, vol. 217, no. 1–2, pp. 145–153, Nov. 1994, doi: 10.1016/0022-3115(94)90314-X.

[15] J. H. Irby, “Private communication.” 2018.

[16] A. Nagy *et al.*, “A multi-species powder dropper for magnetic fusion applications,” *Rev. Sci. Instrum.*, vol. 89, no. 10, p. 10K121, Oct. 2018, doi: 10.1063/1.5039345.

[17] A. Bortolon *et al.*, “Real-time wall conditioning by controlled injection of boron and boron-nitride powder in full tungsten wall ASDEX-Upgrade,” *Nucl. Mater. Energy*, 2018.

[18] R. Lunsford *et al.*, “Active conditioning of ASDEX Upgrade tungsten plasma-facing components and discharge enhancement through boron and boron nitride particulate injection,” *Nucl. Fusion*, vol. 59, no. 12, p. 126034, Dec. 2019, doi: 10.1088/1741-4326/ab4095.

[19] E. J. Doyle *et al.*, “Demonstration of ITER operational scenarios on DIII-D,” *Nucl. Fusion*, vol. 50, no. 7, p. 75005, 2010, [Online]. Available: http://stacks.iop.org/0029-5515/50/i=7/a=075005.

[20] R. Lunsford *et al.*, “Multi-species impurity granule injection and mass deposition

projections in NSTX-U discharges," *Nucl. Fusion*, vol. 57, no. 7, p. 076008, Jul. 2017, doi: 10.1088/1741-4326/aa6cd3.

[21] C. M. Samuell *et al.*, "Verification of Doppler coherence imaging for 2D ion velocity measurements on DIII-D," *Rev. Sci. Instrum.*, vol. 89, no. 9, p. 093502, Sep. 2018, doi: 10.1063/1.5039367.

[22] A. Bortolon *et al.*, "Real-time wall conditioning by controlled injection of boron and boron nitride powder in full tungsten wall ASDEX Upgrade," *Nucl. Mater. Energy*, vol. 19, pp. 384–389, May 2019, doi: 10.1016/J.NME.2019.03.022.

[23] C. P. C. Wong *et al.*, "Divertor and midplane materials evaluation system in DIII-D," *J. Nucl. Mater.*, vol. 363–365, pp. 276–281, Jun. 2007, doi: 10.1016/J.JNUCMAT.2007.01.121.

[24] A. Loarte *et al.*, "Progress on the application of ELM control schemes to ITER scenarios from the non-active phase to DT operation," *Nucl. Fusion*, vol. 54, no. 3, p. 33007, 2014, [Online]. Available: http://stacks.iop.org/0029-5515/54/i=3/a=033007.

[25] P. B. Snyder *et al.*, "Edge localized modes and the pedestal: A model based on coupled peeling-ballooning modes," *Phys. Plasmas*, vol. 9, no. 5, pp. 2037–2043, May 2002, doi: http://dx.doi.org/10.1063/1.1449463.

[26] G. Haas and H.-S. Bosch, "In vessel pressure measurement in nuclear fusion experiments with asdex gauges," *Vacuum*, vol. 51, no. 1, pp. 39–46, Sep. 1998, doi: 10.1016/S0042-207X(98)00131-6.

[27] R. J. Fonck, A. T. Ramsey, and R. V Yelle, "Multichannel grazing-incidence spectrometer for plasma impurity diagnosis: SPRED," *Appl. Opt.*, vol. 21, no. 12, pp. 2115–2123, Jun. 1982, doi: 10.1364/AO.21.002115.

[28] E. A. Unterberg *et al.*, "Global particle balance measurements in DIII-D H-mode discharges," in *Journal of Nuclear Materials*, Aug. 2011, vol. 415, no. 1 SUPPL, pp. S740–S747, doi: 10.1016/j.jnucmat.2011.02.028.

[29] C. P. . Wong, D. . Whyte, R. . Bastasz, J. Brooks, W. . West, and W. . Wampler, “Divertor materials evaluation system (DiMES),” *J. Nucl. Mater.*, vol. 258–263, pp. 433–439, Oct. 1998, doi: 10.1016/S0022-3115(98)00407-3.

[30] D. L. Rudakov *et al.*, “Plasma interactions with the outboard chamber wall in DIII-D,” *J. Nucl. Mater.*, vol. 390–391, no. 1, pp. 785–788, Jun. 2009, doi: 10.1016/j.jnucmat.2009.01.208.

[31] J. D. Duran, E. A. Unterberg, M. P. Zach, W. R. Wampler, D. L. Rudakov, and D. C. Donovan, “Multiple Analytical Approach to Isotopic Transport Analysis in Magnetic Fusion Devices,” *Fusion Sci. Technol.*, pp. 1–6, May 2019, doi: 10.1080/15361055.2019.1610316.

[32] F. J. Domínguez-Gutiérrez *et al.*, “Unraveling the plasma-material interface with real time diagnosis of dynamic boron conditioning in extreme tokamak plasmas,” *Nucl. Fusion*, vol. 57, no. 8, p. 086050, Aug. 2017, doi: 10.1088/1741-4326/aa7b17.

[33] M. A. Makowski, C. J. Lasnier, A. W. Leonard, J. Boedo, J. G. Watkins, and D. N. Hill, “Comparison of upstream Te profiles with downstream heat flux profiles and their implications on parallel heat transport in the SOL in DIII-D,” in *Journal of Nuclear Materials*, Aug. 2011, vol. 415, no. 1 SUPPL, pp. S357–S359, doi: 10.1016/j.jnucmat.2010.09.039.

[34] M. Saggio, C. Montandon, A. Bourenkov, L. Frey, and P. Pichler, “Distortion of SIMS profiles due to ion beam mixing,” *Radiat. Eff. Defects Solids*, vol. 141, no. 1–4, pp. 37–52, 1997, doi: 10.1080/10420159708211555.

[35] F. Bedoya, J. P. Allain, F. Scotti, B. LaBombard, R. Kaita, and P. S. Krstic, “Effect of boronization on plasma-facing graphite surfaces and its correlation with the plasma behavior in NSTX-U,” *Nucl. Mater. Energy*, vol. 17, pp. 211–216, 2018, doi: 10.1016/j.nme.2018.10.010.

[36] U. Schneider *et al.*, “Boronization of ASDEX,” *J. Nucl. Mater.*, vol. 176–177, no. C, pp. 350–356, Dec. 1990, doi: 10.1016/0022-3115(90)90071-T.

[37] P. S. Krstic, J. P. Allain, F. J. Dominguez-Gutierrez, and F. Bedoya, “Unraveling the surface chemistry processes in lithiated and boronized plasma material interfaces under extreme conditions,” *Matter and Radiation at Extremes*, vol. 3, no. 4. Elsevier B.V., pp. 165–187, Jul. 01, 2018, doi: 10.1016/j.mre.2018.03.003.

[38] J. P. Sharpe, D. A. Petti, and H. W. Bartels, “A review of dust in fusion devices: Implications for safety and operational performance,” *Fusion Eng. Des.*, vol. 63–64, pp. 153–163, Dec. 2002, doi: 10.1016/S0920-3796(02)00191-6.

[39] P. C. Stangeby, “Assessing material migration through 13C injection experiments,” in *Journal of Nuclear Materials*, Aug. 2011, vol. 415, no. 1 SUPPL, pp. S278–S283, doi: 10.1016/j.jnucmat.2010.11.060.

[40] M. Shimada *et al.*, “In-vessel dust and tritium control strategy in ITER,” *J. Nucl. Mater.*, vol. 438, no. SUPPL, 2013, doi: 10.1016/j.jnucmat.2013.01.217.

[41] M. Shoji *et al.*, “Full-torus impurity transport simulation for optimizing plasma discharge operation using a multi-species impurity powder dropper in the large helical device,” *Contrib. to Plasma Phys.*, p. e201900101, Dec. 2019, doi: 10.1002/ctpp.201900101.

[42] F. Nespoli *et al.*, “First impurity powder injection experiments in LHD,” submitted to *Nucl. Mater. Energy*.

Figures

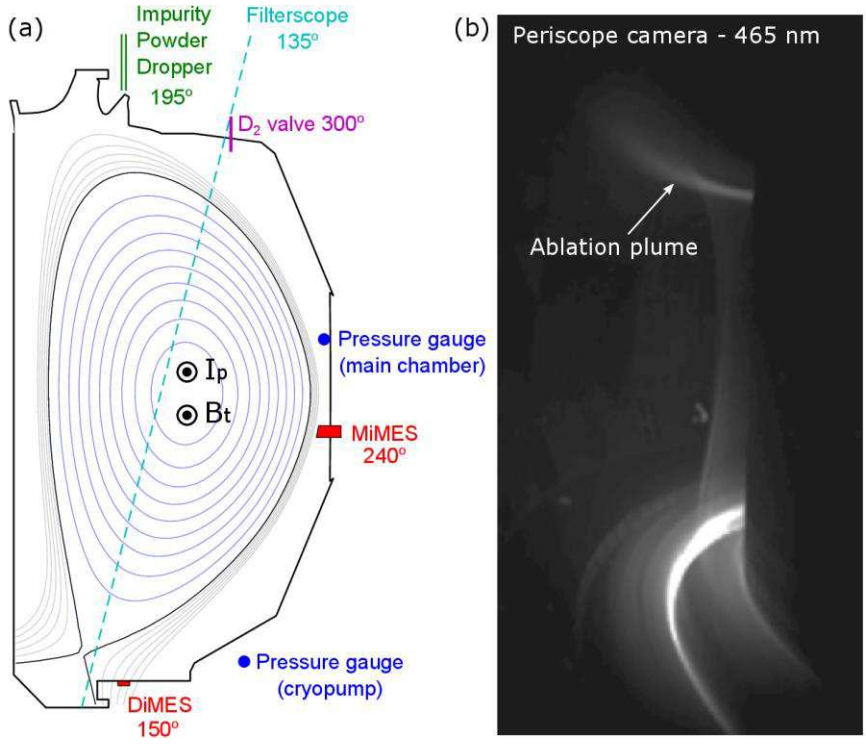

Figure 1. (a) Poloidal cross section of DIII-D magnetic equilibrium utilized for real-time boronization experiments, showing the injection location of the Impurity Powder Dropper, the location of the DiMES and MiMES probes, the pressure gauges and a spectroscopic divertor view, as well as the directions of the plasma current I_p and magnetic field B_t. The angle values annotated refer to the toroidal position of respective components. (b) Wide-angle image of emission at 465 nm showing the plume of B ablation in the upper divertor.

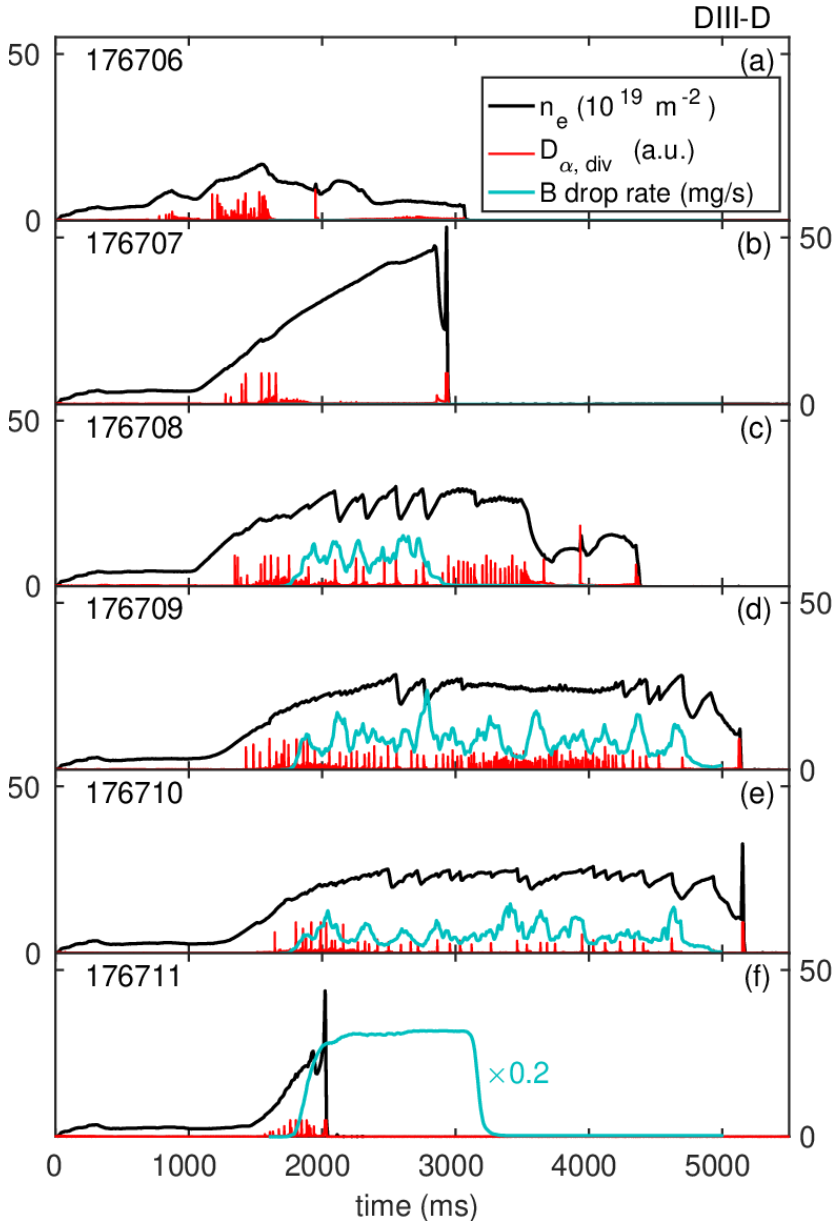

Figure 2. Evolution of line integrated electron density, D_α emission from the lower divertor, and B injection rates. The latter corresponds to the calibrated measurement of the powder flow in the IPD system, illustrated here with an added delay of 0.8 s to account for the free-fall time. The B flow rate in panel (f) is scaled down to 20% of the actual value.

Table 1. Injection parameters for B powder injection in the wall conditioning experiment.

Shot	Rate (mg/s)	Injection interval (s)	B injected	Cumulative B injected	Plasma duration (s)	Time of LH transition
176706	-	-	-	-	2.9	1.050
176707	-	-	-	-	2.9	1.075
176708	10	1 s	10 mg	10 mg	3.6	1.102
176709	10	3 s	30 mg	40 mg	4.9	1.270
176710	8	3 s	24 mg	64 mg	5.0	1.360
176711	155	0.2 s	31 mg	95 mg	2.0	1.480

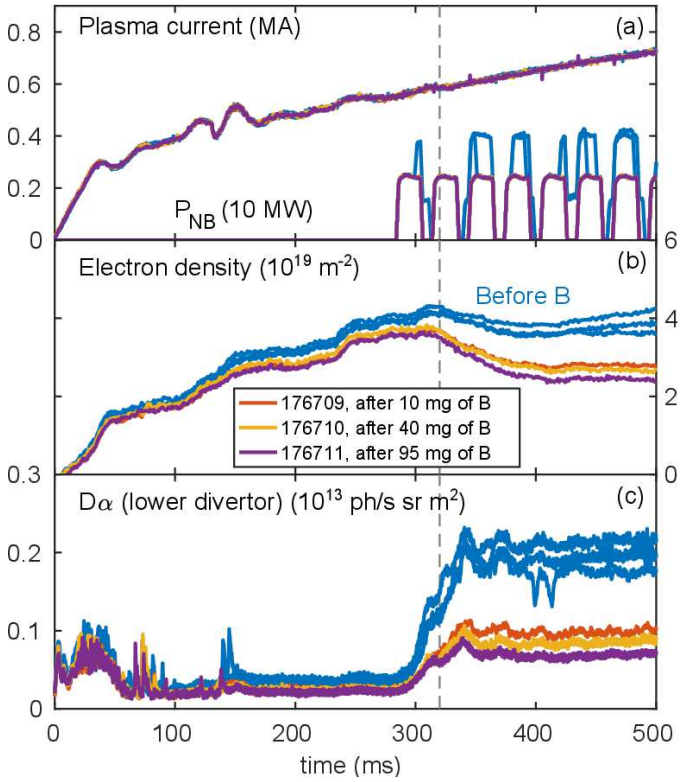

Figure 3. Evolution of (a) plasma current and neutral beam power, (b) line integrated electron density and (c) Balmer-α brightness from a viewchord aimed at the lower divertor for a sequence of plasma discharges before and after B injection. Over the time interval illustrated the plasma is confined in L-mode, transitioning from inner-wall limited to lower single null at t=320 ms.

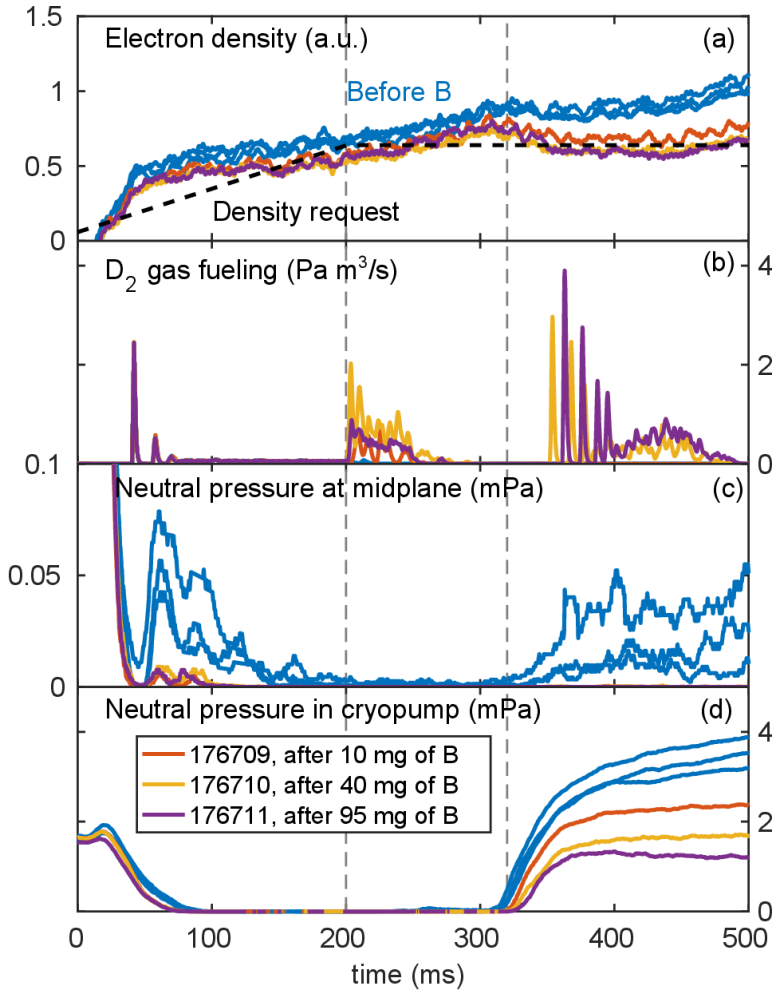

Figure 4. Evolution of (a) plasma density observer compared to the target request, (b) gas injection rate and (c,d) neutral gas pressure measured at the outboard midplane and lower divertor cryo-pump plenum (d). The vertical dashed lines indicate the times when the valve feedback-control is engaged (t=200 ms), and the transition from limited to pumped OSP diverted configuration (t=320 ms).

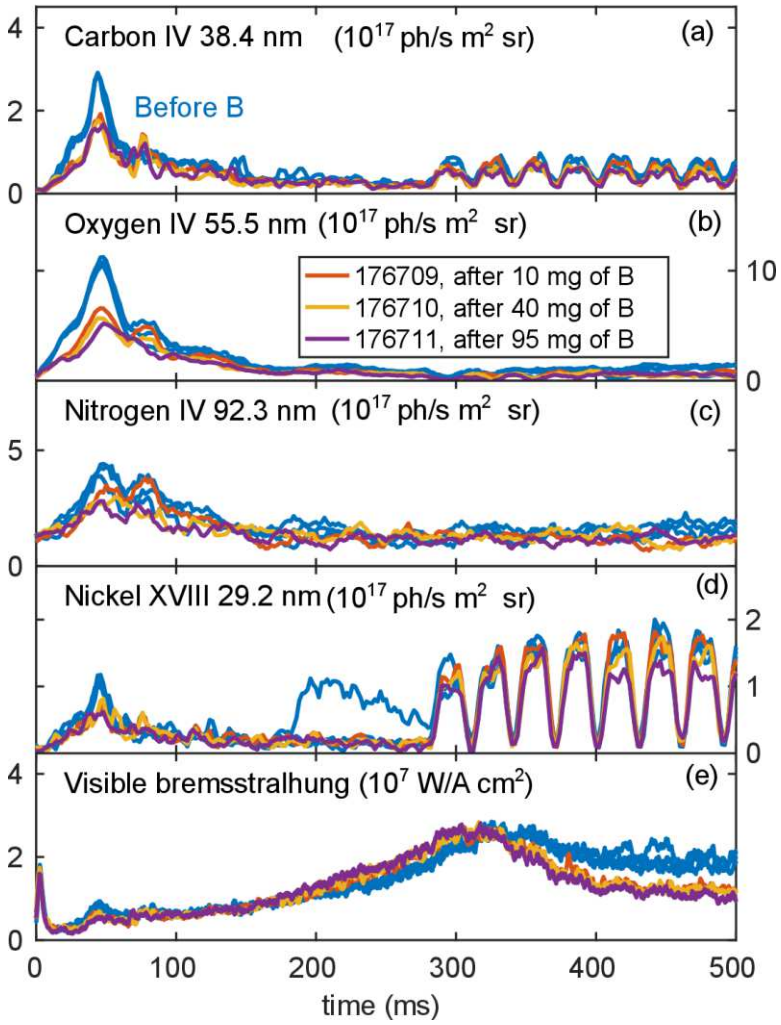

Figure 5. Brightness of selected lines of C, O, N and Ni, measured by the vacuum ultraviolet spectrometer SPRED (a,b,c,d) and line-integrated visible bremsstrahlung emission from a chord intersecting the plasma core (e). The emission peak at t=20-60 ms is associated with discharge breakdown. Pulsing behaviour of C IV and Ni XVII lines after t=300 ms is due to the NBI modulation, indicating a contribution from core-localized charge-exchange emission.

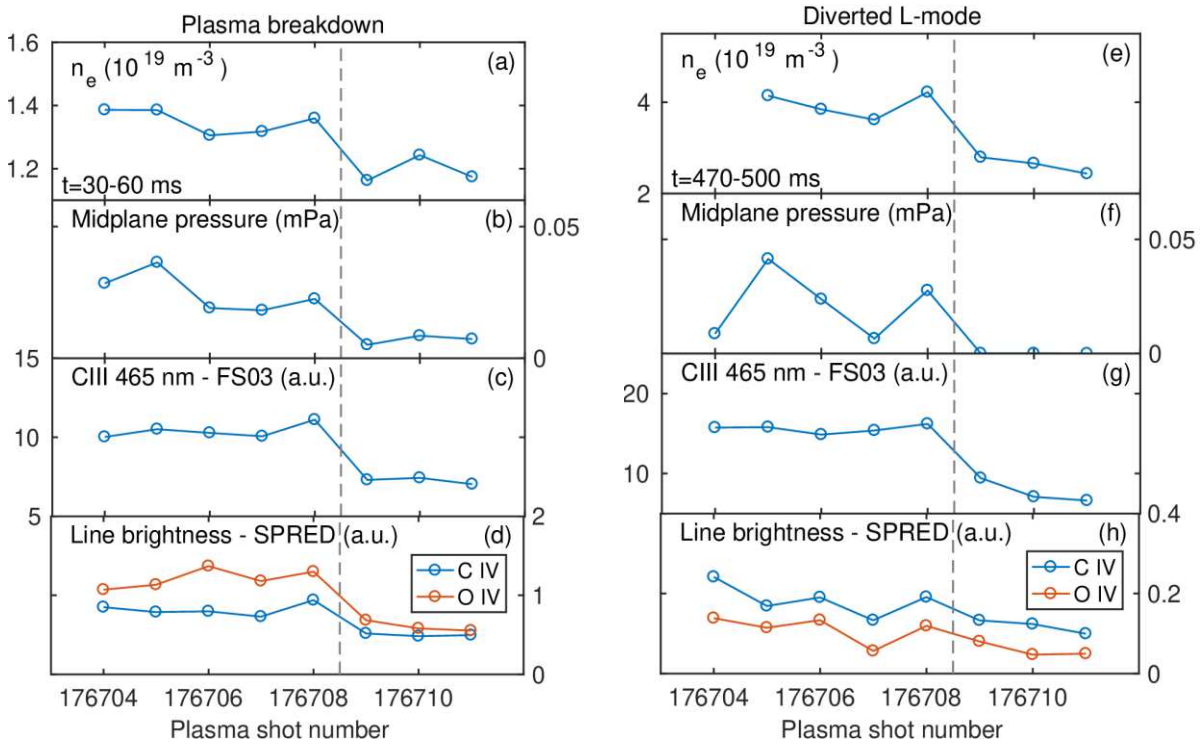

Figure 6. Shot-by-shot evolution of selected quantities measured at the plasma breakdown (a-d) and during the early L-mode phase in diverted configuration (e-h). The vertical line marks the separation between measurements before/after the first B injection in the H-mode phase of shot 176708.

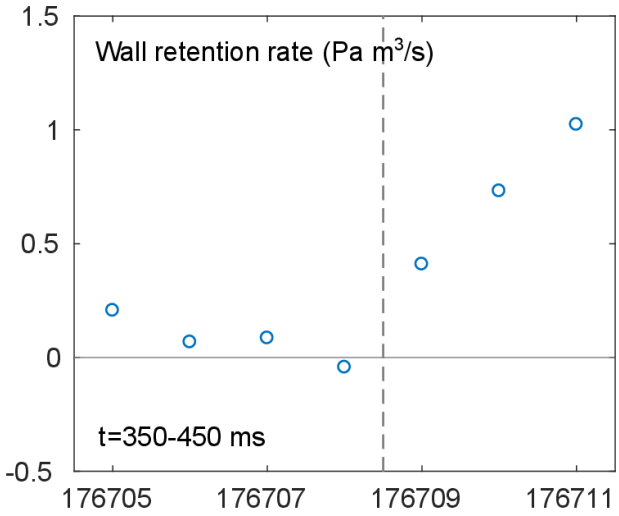

Figure 7. Evolution of D retention rate across the series of plasma discharges, from a dynamical particle balance computation. Data shown correspond to the diverted L-mode time window t=350-450 ms. The vertical line marks the separation between measurements before/after the first B injection in the H-mode phase of shot 176708.

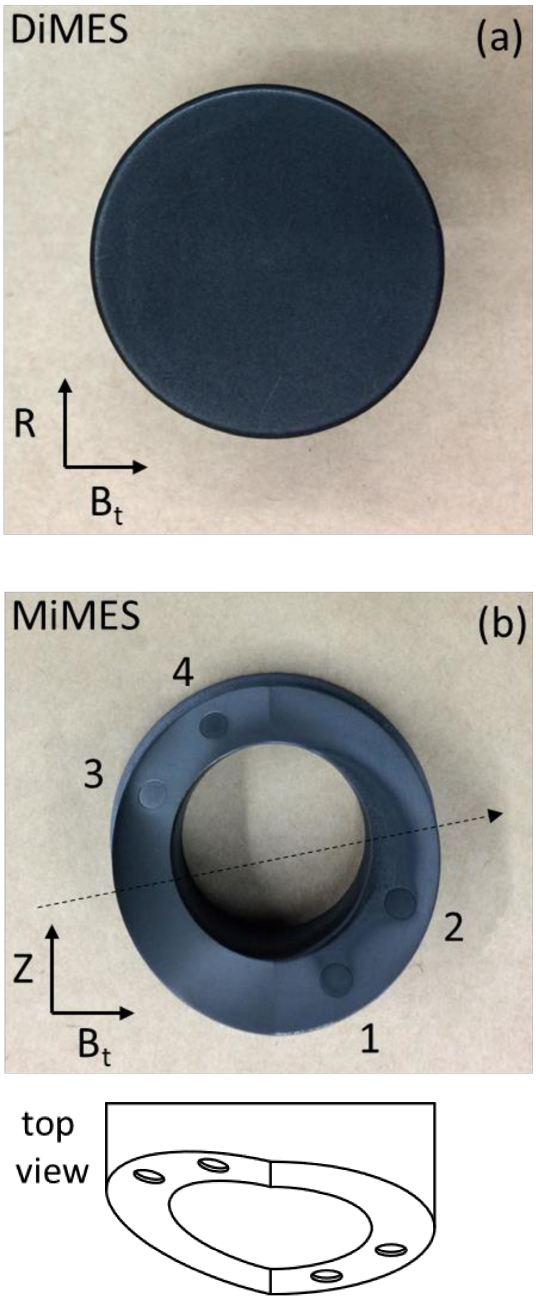

Figure 8. DiMES (a) and MiMES (b) samples after exposure to twelve plasma discharges. The dashed arrow in (b) indicates the orientation of the total magnetic field at the location of the sample head. The schematic presents a top view of the sample geometry.

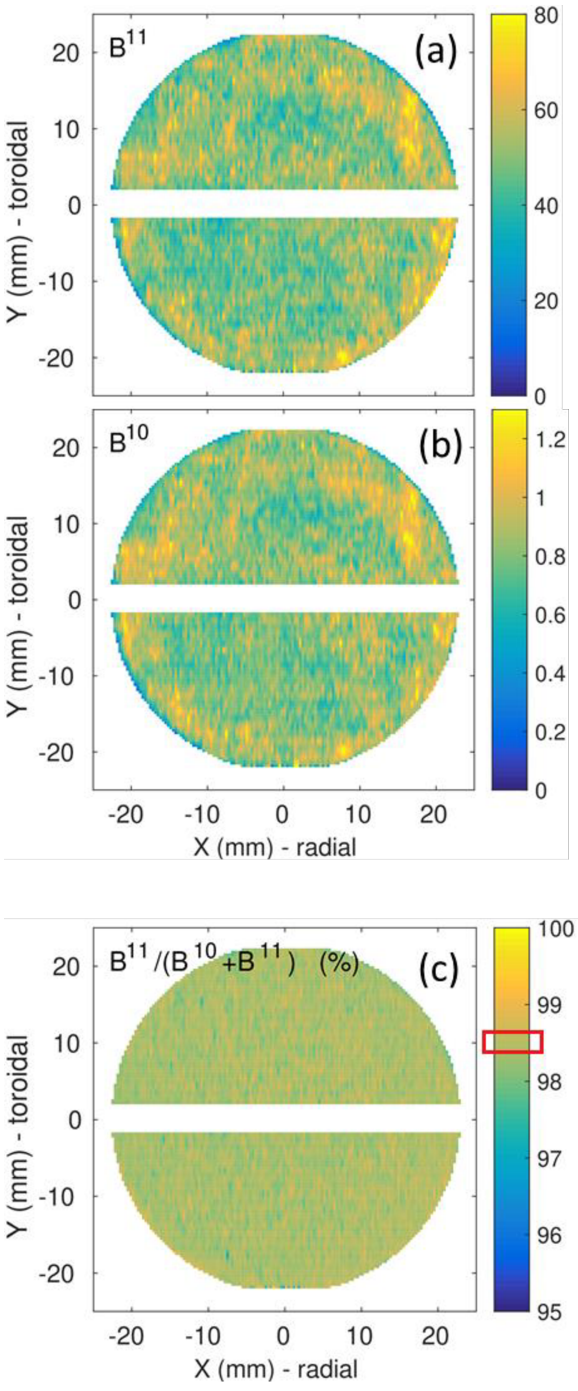

Figure 9. Map of intensity of B^{11} (a) and B^{10} (b) signals on the DiMES sample surface measured with LAMS. The relative concentration of B^{11} (c) indicates an isotope abundance ~98.5%, consistent with the nominal specification of the injected B powder B^{11} >95%.

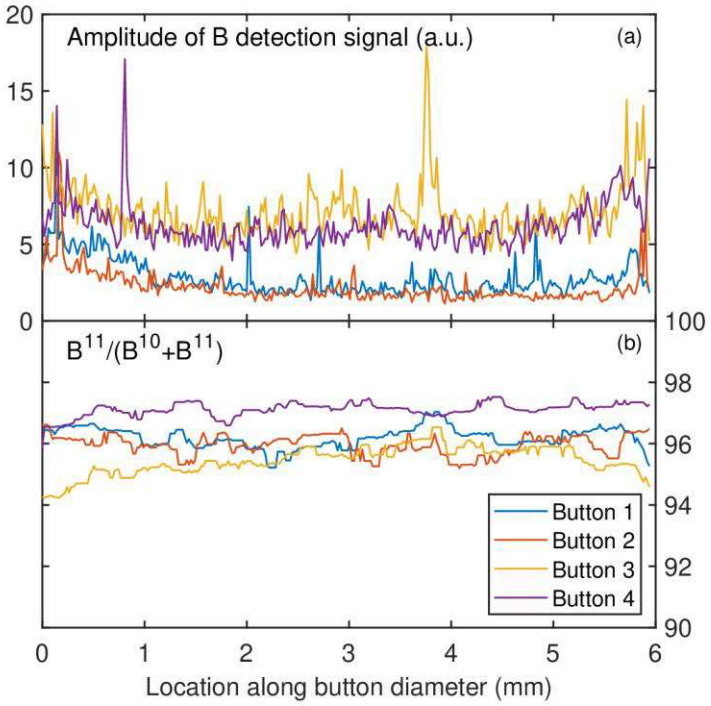

Figure 10. (a) Profile of intensity of mass spectrometer B signal detected from the MiMES samples exposed to downstream (buttons 1 and 2) and upstream (buttons 3 and 4) plasma fluxes. (b) Isotopic concentration of B^{11}>95% found across the samples is consistent with that of the injected B powder.

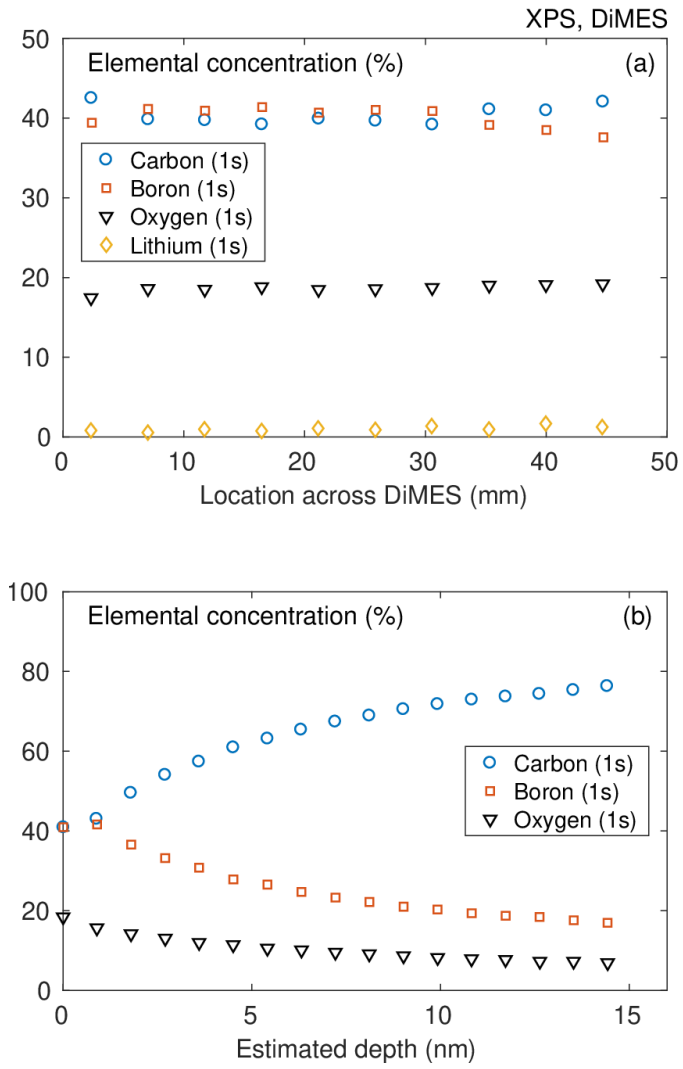

Figure 11. (a) Relative surface abundance of C, B, O and Li measured by x-ray photoelectron spectroscopy (XPS) at ten locations across the DiMES diameter. The transition observed are C(1s) at 284.8 eV, B(1s) at 188.4 eV, O(1s) at 532.6 eV and Li(1s) at 56.1 eV. (b) Relative elemental abundance profile measured at one location after subsequent exposures to an Ar^+ ion beam as a function of the estimated sputtering depth.